

ORIGINAL ARTICLE

A Quadrantic Bias in Prefrontal Representation of Visual-Mnemonic Space

Matthew L. Leavitt^{1,2}, Florian Pieper³, Adam J. Sachs⁴
and Julio C. Martinez-Trujillo^{1,2,5,6,7}

¹Department of Physiology, McGill University, Montreal, Quebec, Canada H3G 1Y6, ²Department of Physiology and Pharmacology, University of Western Ontario, Ontario, Canada N6A 5B7, ³Department of Neuro- & Pathophysiology, University Medical Center Hamburg-Eppendorf (UKE), 20246 Hamburg, Germany, ⁴Division of Neurosurgery, Ottawa Hospital Research Institute, University of Ottawa, Ottawa, Ontario, Canada K19 4E9, ⁵Robarts Research Institute, University of Western Ontario, Ontario, Canada N6A 5B7, ⁶Brain and Mind Institute, University of Western Ontario, Ontario, Canada N6A 5B7 and ⁷Department of Psychiatry, University of Western Ontario, Ontario, Canada N6A 5B7

Address correspondence to Julio C. Martinez-Trujillo, email: julio.martinez@robarts.ca

Abstract

Single neurons in primate dorsolateral prefrontal cortex (dLPFC) are known to encode working memory (WM) representations of visual space. Psychophysical studies have shown that the horizontal and vertical meridians of the visual field can bias spatial information maintained in WM. However, most studies and models have tacitly assumed that dLPFC neurons represent mnemonic space homogeneously. The anatomical organization of these representations has also eluded clear parametric description. We investigated these issues by recording from neuronal ensembles in macaque dLPFC with microelectrode arrays while subjects performed an oculomotor delayed-response task. We found that spatial WM representations in macaque dLPFC are biased by the vertical and horizontal meridians of the visual field, dividing mnemonic space into quadrants. This bias is reflected in single neuron firing rates, neuronal ensemble representations, the spike count correlation structure, and eye movement patterns. We also found that dLPFC representations of mnemonic space cluster anatomically in a nonretinotopic manner that partially reflects the organization of visual space. These results provide an explanation for known WM biases, and reveal novel principles of WM representation in prefrontal neuronal ensembles and across the cortical surface, as well as the need to reconceptualize models of WM to accommodate the observed representational biases.

Key words: meridian effect, microelectrode array recording, neurophysiology, VSTM, working memory

Introduction

Working memory (WM) is the ability to transiently maintain and manipulate information that is no longer available in the environment (Baddeley and Hitch 1974). It is strongly correlated with measures of human intelligence, and a critical foundation for complex behaviors (Fuster 1973; Engle et al. 1999; Miller and Cohen 2001). Sustained neuronal activity in the absence of

stimulus input is considered a neural mechanism for WM (Hebb 2005). Indeed, single neurons in dorsolateral prefrontal cortex (dLPFC) and other regions of the macaque brain exhibit spatially-selective sustained activity during WM maintenance (Fuster and Alexander 1971; Niki 1974; Batuev 1986; Gnadt and Andersen 1988; Funahashi et al. 1989; Constantinidis and Procyk 2004).

Psychophysical studies have shown that maintaining visuospatial information in WM subjects it to stereotyped distortions, or biases. Saccades to remembered target locations show biases in their endpoint distributions that vanish when saccade targets remain visible (White et al. 1994). The horizontal and vertical meridians of the visual field also appear to exert biases on the contents of spatial WM: remembered locations are repelled away from the meridians, towards the center of a quadrant (Huttenlocher et al. 1991, 2004; Merchant et al. 2004; Haun et al. 2005). These results suggest inhomogeneities in the representation of remembered locations across the visual field. However, little is known about how mnemonic representations vary across the visual field. The preponderance of previous studies have parameterized visual space as either binary (e.g., left/right) or unidimensional (e.g., degrees of angle across the same eccentricity) (Funahashi and Kubota 1994; Goldman-Rakic 1995). One study provided examples of dLPFC neurons with non-Gaussian spatial WM fields, but did not further elaborate on the receptive fields' structures (Rainer et al. 1998). Although these studies have substantially advanced our understanding of WM, they have also led to models that assume a continuous and/or homogenous representation of the visual-mnemonic space (Camperi and Wang 1998; Compte et al. 2000; Constantinidis and Wang 2004; Wimmer et al. 2014). This assumption, however, has not been systematically tested.

Recent behavioral and physiological studies examining WM capacity have demonstrated varying degrees of independence between the left and right visual hemifields (Vogel and Machizawa 2004; Delvenne 2005; Buschman et al. 2011; Delvenne et al. 2011). However, these studies treated visual space as a binary variable, thus restricting their ability to make conclusions about visual-mnemonic space beyond that it is represented separately for each hemifield.

Spatial attention is also subject to biases by the meridians of the visual field, which is relevant given the known overlap in neural substrates between attention and WM (LaBar et al. 1999; Awh and Jonides 2001; Constantinidis et al. 2001a; Miller and Cohen 2001; Lebedev et al. 2004; Awh et al. 2006; Postle 2006; Theeuwes et al. 2009; Ikkai and Curtis 2011; Gazzaley and Nobre 2012). Psychophysical research has shown that attentional capabilities seem to be somewhat independent for different visual hemifields (Alvarez et al. 2012) and/or quadrants (Carlson et al. 2007; Liu et al. 2009), and that shifting the focus of attention across a meridian incurs a substantial reaction time penalty (Rizzolatti et al. 1987). It is possible that WM and attentional representations share similar constraints, and therefore WM representations of visual space exhibit hemifield or quadrant biases.

It has also remained ambiguous whether dLPFC contains a topographically organized representation of visual-mnemonic space. There is some evidence that dLPFC is organized in a microcolumnar manner, such that groups of cells within the same ~0.7 mm region share recurrent excitatory connections, while inhibitory connections to other microcolumns extend laterally up to 7 mm (Kritzer and Goldman-Rakic 1995; Rao et al. 1999). Such an organization could result in clustering of spatial mnemonic selectivity, such that during WM maintenance neurons within a cluster encoding the same representation share mutual excitation while inhibiting neurons in other clusters encoding different representations. This, however, has yet to be documented.

In order to address these questions, we recorded from ensembles of single neurons in dLPFC area 8a while subjects performed an oculomotor delayed-response task. We found

that spatial WM representations are biased in a quadrant manner: activity underlying WM for stimuli on the opposite side of a meridian from a neuron's memory field is substantially decreased relative to representations of stimuli on the same side of a meridian. This bias is also present in the structure of correlated variability (i.e., spike-rate or noise correlations) during WM maintenance, and evident in the subjects' behavior, as saccades to remembered locations exhibit a tendency to repel away from horizontal and vertical meridians and attract towards quadrant centers. We also found that dLPFC neurons encoding similar remembered locations tend to cluster anatomically, and that representation of the contralateral hemifield on the cortical surface partially reflects the relative distances between points on the retina, though not in a retinotopic manner.

Materials and Methods

Ethics Statement

The animal care and ethics are identical to those in Leavitt et al. (2013, 2017) and were in agreement with Canadian rules and regulations and were preapproved by the McGill University Animal Care Committee. Animals were pair-housed in enclosures according to Canadian Council for Animal Care guidelines. Interactive environmental stimuli were provided for enrichment. During experimental days, water was restricted to a minimum of 35 mL/kg/day, which they could earn through successful performance of the task. Water intake was supplemented to reach this quantity if it was not achieved during the task and water restriction was lifted during nonexperimental days. The animals were also provided fresh fruits and vegetables daily. Body weight, water intake, as well as mental and physical hygiene were monitored daily. Blood cell count, hematocrit, hemoglobin, and kidney function were tested quarterly. If animals exhibited discomfort or illness, the experiment was stopped and resumed only after successful treatment and recovery. All surgical procedures were performed under general anesthesia. None of the animals were sacrificed for the purpose of this experiment.

Task

The task was identical to Leavitt et al. (2017). Trials were separated into 4 epochs: fixation, stimulus presentation (stimulus), delay, and response (Fig. 1A). The animal initiated a trial by maintaining gaze on a central fixation spot (0.08 degrees²) and pressing a lever; the subject needed to maintain fixation within 1.4° of the spot until cued to respond. The fixation period lasted either 482, 636, or 789 ms, determined randomly at the beginning of each trial. After fixation, a sine-wave grating (2.5 Hz/deg, 1° diameter, vertical orientation) appeared at 1 of 16 randomly selected locations for 505 ms. The potential stimulus locations were arranged in a 4 × 4 grid, spaced 4.7° apart, centered around the fixation point. The stimulus period was followed by a randomly variable delay period of 494–1500 ms. The delay period ended and the response period commenced when the fixation point was extinguished, cuing the animal to make a saccade to the location of the previously presented stimulus and then to release the lever. The animal had 650 ms to respond. Successful completion of the trial yielded a juice reward. The minimum duration between trials was 300 ms. Fixation breaks during the trial or failure to saccade to the target in the allotted time resulted in immediate trial abortion without reward and a delay of 3.5 s before the next trial could be initiated.

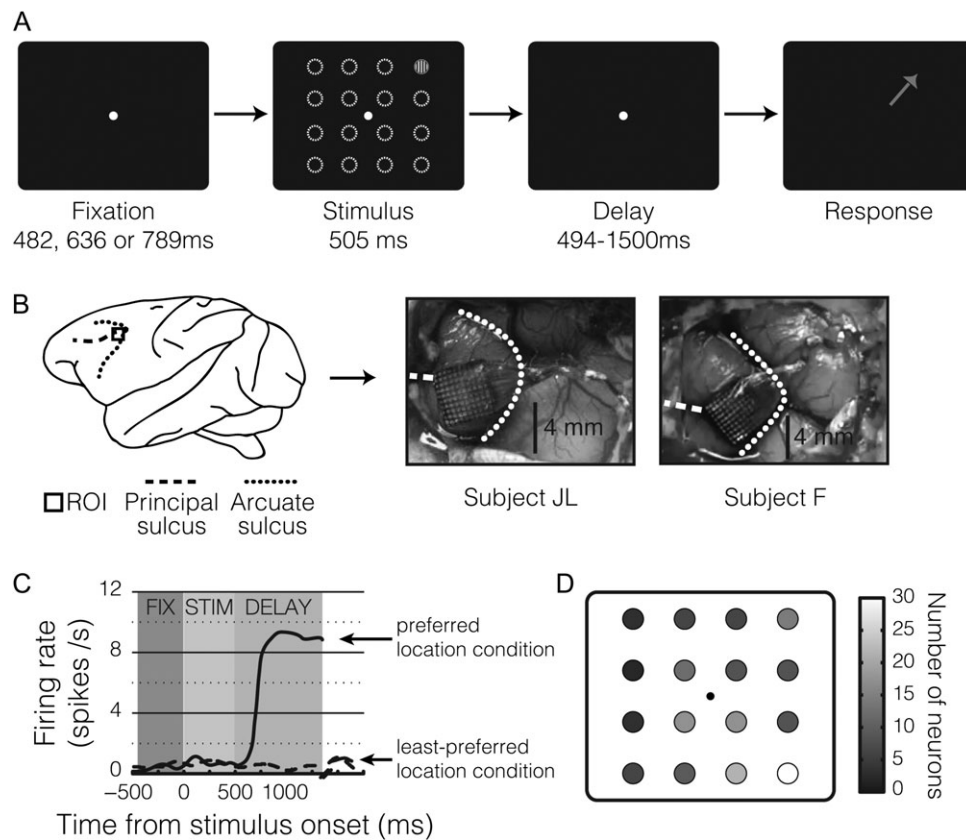


Figure 1. Task, method, and single-cell data. (A) Overview of oculomotor delayed-response task, described in detail in the Methods section. The dashed circles indicating potential cue locations are shown for illustrative purposes and are not present in the task. (B) Array implantation sites and anatomical landmarks in both subjects. (C) Example delay-selective neurons. (D) Distributions of neurons' preferred locations during the delay epoch.

Experimental Setup

The experimental setup is identical to [Leavitt et al. \(2013, 2017\)](#) and [Tremblay et al. \(2014\)](#). The stimuli were back-projected onto a screen located 1 m from the subjects' eyes using a DLP video projector (NEC WT610, 1024 × 768 pixel resolution, 85 Hz refresh rate). Subjects performed the experiment in an isolated room with no illumination other than the projector, which still provides some illumination even when projecting black. Eye positions were monitored using an infrared optical eye-tracker (EyeLink 1000, SR Research, Ontario, Canada) and endpoint centroids were adjusted to match the target location for each session. A custom computer program controlled stimulus presentation and reward dispensation, and recorded eye position signals and behavioral responses. Subjects performed the experiment while seated in a standard primate chair, and were delivered reward via a tube attached to the chair and an electronic reward dispenser (Crist Instruments) that interfaced with the computer. Prior to the experiments, subjects were implanted with head posts. The head post(s) interfaced with a head holder to fix the monkeys' heads to the chair during experiment sessions.

Microelectrode Array Implant

As in [Leavitt et al. \(2013, 2017\)](#), [Tremblay et al. \(2014\)](#), and [Boulay et al. \(2016\)](#), we chronically implanted a 10 × 10, 1.5 mm microelectrode array (MEA; Blackrock Microsystems LLC) ([Maynard et al. 1997](#); [Normann et al. 1999](#)) in each monkey's left dLPFC— anterior to the knee of the arcuate sulcus and

caudal to the posterior end of the principal sulcus (area 8a) ([Fig. 1B](#)). Detailed surgical procedures can be found in [Leavitt et al. \(2013\)](#).

Recordings and Spike Detection

Data were recorded using a “Cerebus Neuronal Signal Processor” (Blackrock Microsystems LLC) via a Cereport adapter. Spike waveforms were detected online by thresholding. The extracted spikes (48 samples at 30 kHz) were resorted manually in “OfflineSorter” (Plexon Inc.). The electrodes on each MEA were separated by at least 0.4 mm and were organized into 3 blocks of 32 electrodes (A, B, and C). We collected data from one block during each recording session. Detailed recording procedures can be found in [Leavitt et al. \(2013\)](#).

Analysis Epochs

We analyzed the final 483 ms of the fixation epoch and the entirety of the stimulus epoch; we analyzed the entire delay epoch after the first 150 ms in order to minimize the potential impact of signal latency and stimulus aftereffects ([Mendoza-Halliday et al. 2014](#)). We only analyzed successfully completed trials. Data analysis was performed using MATLAB and SPSS.

Single Unit Yield and Epoch Selectivity

We collected spike data from a total of 201 single neurons (99 in JL and 102 in F) from 70 unique recording sites (24 in JL and

46 in F) across 15 recording sessions (7 in JL and 8 in F). To determine whether a neuron was spatially tuned for the stimulus location during the stimulus or delay epochs, we computed a Kruskal–Wallis one-way analysis of variance on the average firing rates with location as the factor. Tuned neurons showed at least one location with a significantly different firing rate ($P < 0.05$). We found 143 of 201 (71%) neurons exhibited stimulus selectivity and 157 (78%) exhibited delay selectivity (Fig. 1C, D, Supplementary Fig. S1B,C), yielding 902 correlation pairs between delay-selective units. A neuron’s preferred location was defined as the location that elicited the largest response during the epoch of interest.

Spatial Autocorrelation Analysis

To determine whether delay epoch selectivity is anatomically clustered, we first determined the preferred memory location of the parcel of cortex around each electrode on the microelectrode array, which we defined as the remembered location that generated the greatest response of all thresholded activity on that electrode, across all recording sessions. This yielded a single preferred location for each electrode on the array. Next, we computed Moran’s I (Moran 1950; Bullock et al. 2017; Zuur et al. 2007) across the entire array. Moran’s I is a measure of spatial autocorrelation—the degree of clustering or similarity among objects in space—defined as:

$$I = \frac{N}{\sum_i \sum_j w_{ij}} \frac{\sum_i \sum_j w_{ij} (X_i - \bar{X})(X_j - \bar{X})}{\sum_i (X_i - \bar{X})^2},$$

where N is the number spatial units indexed by i and j ; X is the variable of interest; \bar{X} is the mean X ; and w_{ij} is an element of a matrix of spatial weights. Values of I range from -1 to 1 . Positive values of Moran’s I indicate that similar feature values are spatially clustered, while negative values of Moran’s I indicate that similar feature values are spatially repellant or dispersed. Moran’s I was computed iteratively, extending the radius of included locations (the spatial radius) each time, until the whole array was included. This allowed us to determine how preferred location similarity clusters across different spatial scales. For example, computing Moran’s I for the smallest cluster radius (400 μm) only included adjacent units, while computing it for the largest cluster radius included all units on the array. This was performed separately for the horizontal and vertical components of the preferred location, and the results were averaged. Significance was assessed using permutation tests.

Single Unit Firing Rate Meridian Effects

In order to test whether single neurons’ firing rates were significantly biased by meridians, we first computed the mean response of each selective neuron to each stimulus location for the epoch of interest. Next, we z-scored each neuron’s 16 mean responses to yield standardized firing rates that could be compared across neurons. Finally, we calculated whether a neuron’s firing rates were significantly lower for locations that lie across a meridian from that neuron’s preferred location, relative to equidistant neurons that fall within the same quadrant as the preferred location. The comparison intervals between group medians in Figure 3, Supplementary Figures S2–S4, S8, and S9 are defined as the median $\pm 1.57(q_3 - q_1)/\sqrt{n}$, where q_3 is the 75th percentile and q_1 is the 25th percentile.

In order to control for the difference in the proportion of intraquadrant versus extraquadrant locations relative to the preferred locations (Fig. 3A,C; there are 2 extraquadrant diagonal locations vs. only one intraquadrant diagonal location), we randomly subsampled half of the diagonal extraquadrant locations such that the number of diagonal intraquadrant and extraquadrant locations were matched. This procedure was repeated 5000 times to obtain a bootstrapped distribution of the median extraquadrant response. This distribution of median values was then compared with the median intraquadrant response.

Stepwise Regression

The distance between stimulus locations covaries with other factors, such as eccentricity and angle. In order to test whether the observed quadratic biases in single neuron firing rates could be ascribed to these covarying factors, we performed a stepwise linear regression ($P_{\text{entry}} = 0.05$, $P_{\text{removal}} = 0.1$) to determine which factors significantly affect single neuron firing rates. The regression equation is of the form:

$$y = \beta_0 + \beta_D D + \beta_\theta \theta + \beta_E E + \beta_H H + \beta_V V + \beta_{D\theta} D\theta + \beta_{DE} DE + \beta_{DH} DH + \beta_{DV} DV + \beta_{\theta E} \theta E + \beta_{\theta H} \theta H + \beta_{\theta V} \theta V + \beta_{EH} EH + \beta_{EV} EV + \beta_{HV} HV.$$

where y is the delay epoch firing rate, β_0 is the constant (intercept term), D is the Euclidean distance between the remembered location and preferred location, θ is the angle between the remembered location and the preferred location, E is the difference in eccentricity between the remembered location and the preferred location, H is whether the remembered location is across a horizontal meridian from the preferred location, and V is whether the remembered location is across a vertical meridian from the preferred location. The full model is thus composed of a constant, each of the primary factors listed above, and all the first-order interaction terms. In order to control for collinearity, we determined whether the variance inflation factor (VIF) of any coefficients in the final model were greater than 10. If so, we removed the coefficient with largest VIF and repeated the stepwise regression. This procedure was repeated until all coefficients in the final model had a VIF less than 10. The coefficients removed due to collinearity were $\beta_{D\theta}$, $\beta_{\theta H}$, β_{DH} , $\beta_{\theta V}$, β_{DE} , and β_{DV} .

Quadratic Bias Visualization

In order to visualize the quadratic bias and obtain a continuous estimate of each neuron’s response to the entire region of the visual field covered by the stimulus array, we fit a surface to each neuron’s delay-epoch activity for the 16 stimulus locations (Fig. 4). Specifically, we computed the mean firing rate for each of the 16 locations, then fit a 2D, second-order polynomial of the form

$$f(x, y) = p_{0,0} + p_{1,0}x + p_{0,1}y + p_{2,0}x^2 + p_{0,2}y^2 + p_{1,1}xy$$

to the x - and y -coordinates of each stimulus location. This yielded a function we refer to as the “response surface.” Other than the location of the function’s peak, the firing rate variability represented across the response surfaces was only used for visualization purposes and not for quantitative analysis.

Correlation (r_{sc}) Analysis

In order to compute r_{sc} , we first calculated the z-scores of each unit's spike counts for each condition (i.e., stimulus location). This removes the spike-rate variability across conditions due simply to variability in firing rate responses to different stimuli (i.e., stimulus selectivity) and differences in baseline firing rates for different neurons. We then grouped units into simultaneously recorded pairs ($n = 1319$) and computed Pearson's correlation coefficients ($r_{sc,raw}$) between the z-scored spike counts during each task epoch (Cohen and Kohn 2011; Leavitt et al. 2013, 2017). In addition, we minimized the risk of falsely inflating the correlation values by excluding correlations between units on the same electrode from analysis. Fisher's r -to- z transformation was applied to the correlation coefficients in order to stabilize the variance for hypothesis testing. We also calculated correlations after shuffling the spike rates for all trials (Averbeck and Lee 2006; Cohen and Kohn 2011; Tremblay et al. 2014; Leavitt et al. 2017). The shuffling procedure consisted of randomizing the trial order within each location condition for each neuron, then computing the spike count correlation ($r_{sc,shuff}$). This procedure destroys the simultaneity in the recordings, thereby providing a measure of the magnitude of correlations expected by chance. The shuffling was repeated 1000 times. The mean of the 1000 shuffles was subtracted from the corresponding $r_{sc,raw}$ to yield a corrected value, henceforth referred to as r_{sc} .

Population Decoding

We used a support vector machine (SVM; Libsvm 3.14 (Chang and Lin 2011)), a linear classifier, to extract task-related activity from the population-level representations of simultaneously recorded neural ensembles (Cortes and Vapnik 1995; Chang and Lin 2011; Moreno-Bote et al. 2014; Tremblay et al. 2014; Boulay et al. 2016; Leavitt et al. 2017). The SVM was given firing rate data from an ensemble in order to predict at which of the 16 locations the stimulus was presented for a given trial, during each of the fixation, stimulus, and delay epochs. The classification was performed separately for each session, using the epoch-averaged firing rates (see Analysis Epochs) of each simultaneously recorded neuron. We normalized each unit's firing rates across all trials by subtracting its midrange rate value and dividing by its range (maximum–minimum), in order to prevent units with larger absolute changes in firing rate from dominating the classification boundaries. These 2 parameters were determined from the training set and applied to both the training and testing sets. We assessed the classifier's performance using cross-validation: a technique in which some proportion of the trials are used to train the decoder, and the decoder attempts to classify the remaining trials. We trained the decoder on 80% of the trials and tested on the remaining 20%. This procedure was repeated such that every trial would be represented once in the testing set. In order to determine whether ensemble representations are biased by meridian effects, we then computed the probability of the decoder mistakenly decoding the remembered location as falling within the same quadrant as the true location and compared it to the probability that the decoder mistakenly decodes the remembered location as being at an equidistant but extraquadrant location from the true location.

Saccade Endpoint Distribution Variability

The variability of saccade endpoint distributions for each target location was computed using an elliptic bivariate normal distribution as in Merchant et al. (2004) (Fig. 7). The ellipse was

centered at the x - y mean of the saccade endpoints for a given target location. We obtained the 2 axes of the ellipse via eigen-decomposition of the covariance matrix of the x - y eye positions (i.e., a matrix in which rows = trials, column 1 = x -position, and column 2 = y -position). The resultant orthogonal eigenvectors are the major and minor axes of the ellipse, and are scaled by the square root of their eigenvalues (the variance) and thus lie along the axes of greatest variability of the data. We scaled the axes by the upper 95th percentile of the χ^2 distribution in order to create an ellipse that contains the central 95% of the saccade endpoint distribution. The orientation of the ellipse is the arctangent of the x and y components of the eigenvector from the major axis (i.e., the larger eigenvector).

Results

Two adult *Macaca fascicularis* performed an oculomotor delayed-response task (Fig. 1A) while we recorded from neural ensembles in dLPFC area 8a using chronically implanted 96-channel micro-electrode arrays (Fig. 1B). The neural correlates of WM for spatial locations have been extensively documented in this brain region (Funahashi 2006; Riley and Constantinidis 2015). The target stimulus could appear at any 1 of 16 possible locations, arranged in a uniformly spaced 4×4 grid around a central fixation point. We collected spike data from a total of 201 single neurons across 15 recording sessions, out of which 157 (78%) exhibited delay-epoch spatial selectivity ($P < 0.05$, Kruskal-Wallis; firing rate \times location; Fig. 1C, Supplementary Fig. S1). A neuron's preferred location was defined as the location that elicited the largest response averaged over the delay epoch (Fig. 1D, Supplementary Fig. S1). Both subjects made incorrect choices about the stimulus location in $<1\%$ of completed trials.

Anatomical Topography of Mnemonic Representations in dLPFC

One outstanding question in studies of spatial WM is whether the dLPFC contains a topographically organized representation of mnemonic space and whether such a representation follows a retinotopic scheme. In order to answer this question, we first determined the memory location that elicited the largest delay-epoch activity in the cortex surrounding each electrode (a "cortical parcel"—see Methods), and defined this as the preferred location for that electrode (Fig. 2A). We then computed Moran's I , a measure of spatial autocorrelation (see Methods), across the range of all distances between electrodes on the array, allowing us to determine how similarity in preferred location clusters across different spatial scales for each subject (Fig. 2B). Positive values of Moran's I indicate that similar feature values are spatially clustered; a given location in space is more likely to be in a local neighborhood with other similar values. Negative values of Moran's I indicate that similar feature values are spatially repellent or dispersed; a given location is more likely to be in a neighborhood with dissimilar values.

Our analysis showed that preferred locations are significantly spatially autocorrelated at distances ≤ 1.5 mm in both subjects ($P < 0.001$ in both subjects, permutation test; Fig. 2B); a given cortical parcel is more likely to be surrounded by other parcels that have similar delay epoch selectivity than by parcels that have dissimilar delay epoch activity. We also found a correlation between anatomical distance between parcels and the Euclidean distance between the preferred memory locations of those parcels, but only for parcels that have preferred memory locations in the contralateral (right) hemifield to the

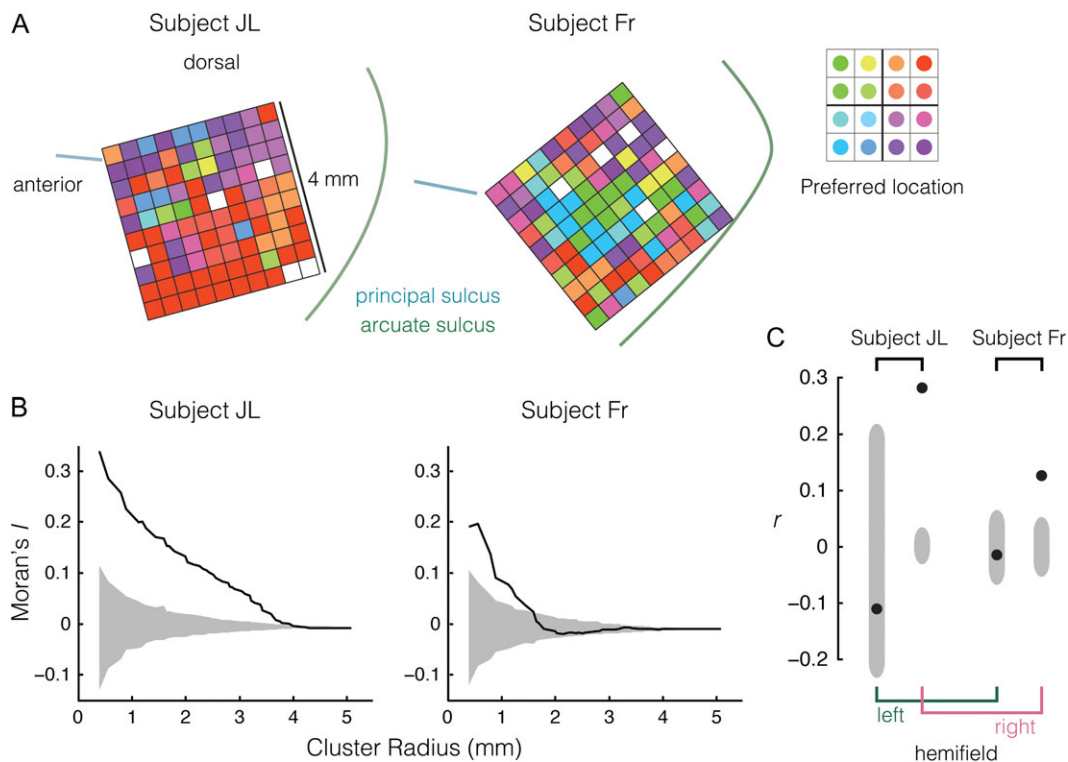


Figure 2. Delay selectivity is anatomically clustered in dLPFC. (A) Preferred memory location of the cortical parcel around each electrode of the microelectrode arrays for subjects JL (left) and FR (right). Preferred memory location was defined as the location eliciting the maximum response of all thresholded activity on an electrode. (B) Moran's I (y -axis) across spatial scales (x -axis) for each subject. Moran's I is a measure of spatial autocorrelation (i.e., clustering) that ranges between -1 and 1 . Positive values of Moran's I indicate that similar preferred locations are spatially clustered. Negative values indicate that similar preferred locations are spatially repellant. Moran's I is computed across the range of all distances between electrodes on the array. The "cluster radius" is maximum distance between units included in the computation. For example, computing Moran's I for the smallest cluster radius (400 mm) only includes adjacent electrodes. Shaded region indicates central 95% of null distribution generated by permutation test, thus any point outside the shaded region is considered significant. Preferred locations are significantly spatially autocorrelated at distances ≤ 1.5 mm in both subjects. (C) Correlation between anatomical distance between cortical parcels, and Euclidean distance between parcels' preferred locations (i.e., Mantel test), computed separately for each visual hemifield and subject. The black point represents the observed value, while the shaded region indicates the central 95% of the null distribution generated by a permutation test. Thus, the correlation is significant for both subjects in the right (i.e., contralateral) hemifield but not the left hemifield.

recording sites ($r = 0.28$, $P < 0.001$, subject JL; $r = 0.13$, $P < 0.001$, subject FR; Mantel Test; Fig. 2C). The correlation was not significant for parcels with selectivity in the ipsilateral/left hemifield ($r = -0.11$, $P = 0.17$, subject JL; $r = -0.02$, $P = 0.33$, subject FR; Mantel Test). These results indicate that the relative spatial relationships in the retina are partially preserved in the cortical surface. However, retinal coordinates do not strictly map onto cortex (e.g., we found no single foveal region), nor is the effect uniform. Indeed, simple inspection of the data in Figure 2A shows that clusters of electrodes with different spatial selectivities (e.g., neurons selective for different hemifields, or for opposite locations in the same hemifield) can sometimes be close, or even adjacent to one another. Thus memory fields in dLPFC exhibit topography, but in a different form than the retinotopic organization of visual areas such as V1 and the FEF.

Spatial Bias in Single Neuron Firing Rates

To determine whether dLPFC neurons represent visual space homogeneously, we first examined how delay activity changed when remembering locations "within" versus "between" quadrants of the visual field. For each neuron with a preferred location adjacent to both a horizontal and vertical meridian (Fig. 3A, B, gray circles, see Methods), we examined delay activity in trials in which stimuli were remembered at locations equidistant from

the preferred location. These locations could fall within the same quadrant as a neuron's preferred location (intraquadrant; Fig. 3A, green circles), or across a meridian (extraquadrant; Fig. 3A, red circles). We found that delay epoch activity was significantly lower for remembered extraquadrant stimuli when compared with equidistant intraquadrant remembered stimuli for neurons that preferred one of the central 4 stimulus locations ($P < 10^{-10}$, bootstrap test—see Methods, Fig. 3A). We then examined each pairing of intra- and extraquadrant locations. The quadrant bias was significant for both the vertical and horizontal meridians, and was not due to differences in eccentricity between remembered locations, or dominated by a single meridian (Fig. 3B). Quadrantic biases for neurons with more eccentric preferred locations showed a similar trend, though not significantly for the horizontal meridian (Supplementary Fig. S2). In order to control for the possibility that the same neurons were recorded from repeatedly across multiple sessions, the same analyses were repeated including only one session per block of recording electrodes (see Methods), yielding a similar trend (Supplementary Fig. S3).

In order to determine whether the bias is exclusively present during the delay period or also exists during visual stimulus input, we applied the same analysis to the firing rates during the stimulus epoch. We found that the quadrant bias during the stimulus epoch was present, though weaker than during the

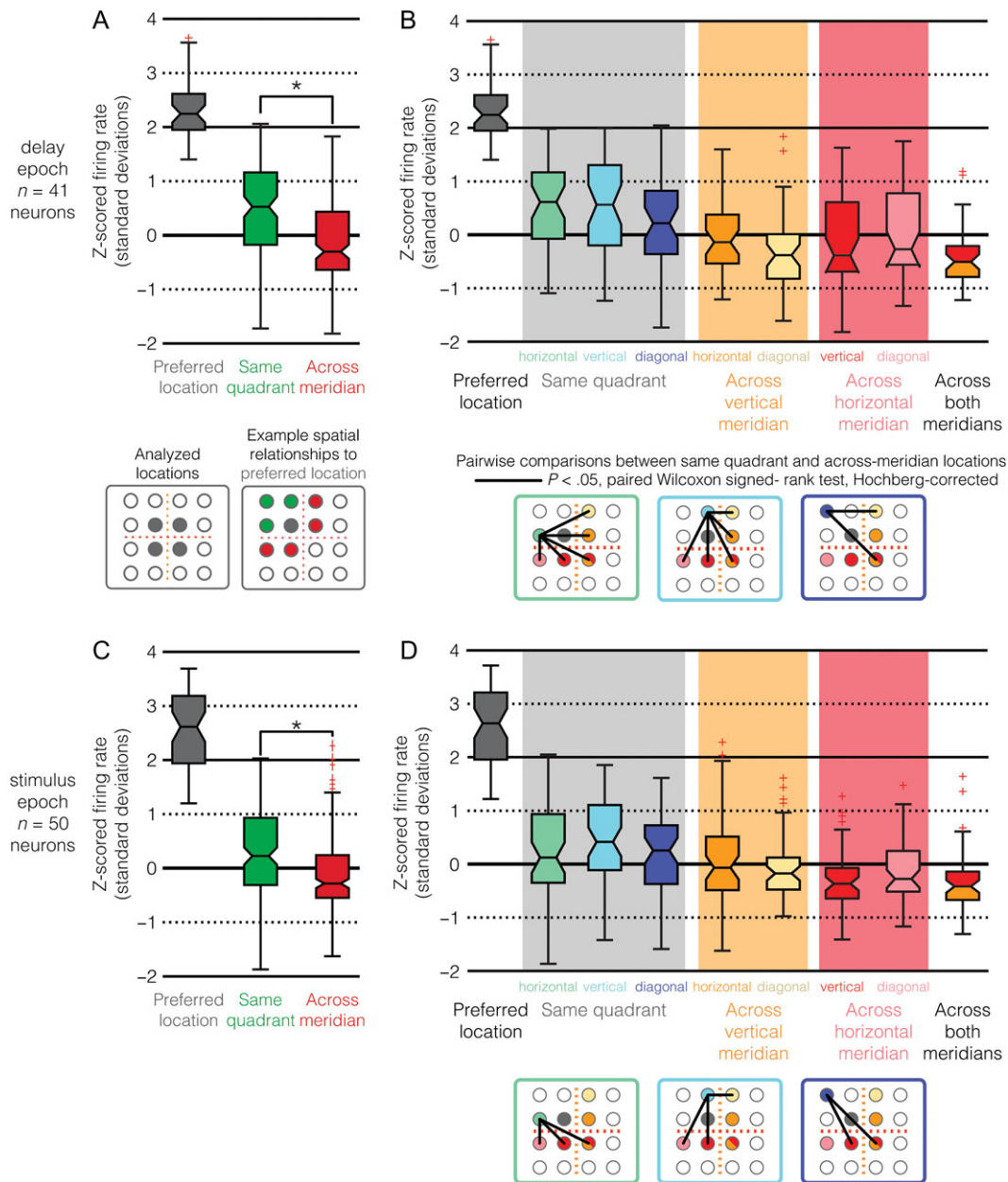


Figure 3. Quadrantic bias in single neuron firing rates. (A) Quadrantic bias in single neuron firing rates (y-axis) pooled across preferred (grey), intraquadrant (green), and extraquadrant (red) locations during the delay epoch. Firing rates are z-scored across all 16 locations. $n = 41$ neurons. $*P < 10^{-10}$, bootstrap test—see Methods. Notches indicate 95% comparison intervals of the median (see Methods). Edges of boxes extend one quartile from median. Whiskers extend to -99.3% distribution coverage. Red crosses indicate outlying values. Only the delay epoch and neurons with preferred locations in the central 4 locations are analyzed in this figure. (B) Similar to (A), but each location lying adjacent to a neuron’s preferred location is presented individually. The spatial relationships to the preferred location and significance of pairwise comparisons are depicted in the legends below the figure. Note that the spatial relationships depicted in the legends are relative; the legends use 1 of the 4 analyzed preferred locations as an example and neurons with preferred locations at each of the 4 central locations are analyzed. (C) Identical to (A), but during the stimulus epoch. $n = 50$ neurons. (D) Identical to (B), but during the stimulus epoch. Note that there are fewer significant differences between responses to intraquadrant versus extraquadrant locations.

delay epoch; there were fewer significant differences in firing rate between intra- versus extraquadrant stimulus locations during stimulus presentation (Fig. 3C,D; Supplementary Fig. S4). This difference was most pronounced for the central 4 preferred locations: 12 of the potential 15 pairs of locations were significantly different during the delay epoch, when compared with 8 of 15 during the stimulus epoch ($P < 0.05$, paired Wilcoxon signed-rank test, Hochberg-corrected; Fig. 3B,D).

Examining the stimulus array, one can see that a number of additional factors, such as eccentricity and angle, may covary with the Euclidean distance between stimuli. Thus, it is possible that these factors are responsible for the observed quadrantic biases in single neuron firing rates during the delay epoch. We assessed this possibility by performing a stepwise linear regression to determine which factors significantly affect single neuron firing rates. Our model attempted to predict the delay

epoch firing rates using the following factors: Euclidean distance of remembered location from preferred location; angular distance from preferred location; eccentricity difference from preferred location; crossing of the vertical meridian; crossing of the horizontal meridian; and all the first-order interaction terms; collinear terms were also removed (see Methods). The horizontal meridian crossing and vertical meridian crossing terms (as well as the rest of the primary factors and multiple interaction terms—see Table S5 for the full results of the analysis) were significant in the final model ($P < 0.001$ for all primary factors), indicating that crossing a meridian significantly influences firing rates, and that the observed quadratic biases cannot be ascribed to alternative covarying factors. To better convey the quadratic bias in firing rates, we visualized how the mnemonic activity of single neurons varies across all 16 remembered locations. We did this by fitting a 2D, second-order polynomial to the firing rates for each of the 16 locations (see Methods; Fig. 4A). The resulting surface approximates the location of maximum activity (the “response peak”) for neurons that respond with similar intensity to multiple adjacent locations, and also provides a continuous estimation of the neuron’s response to the portion of the visual field covered by the stimulus array. The neuron in Figure 4A has a preferred location in the lower right quadrant. The epicenter of the preferred field is within the quadrant, far from the horizontal meridian. We superimposed the response surfaces of multiple example neurons in Figure 4B. The quadratic bias in firing rates is clearly visible in the restriction of neural activity to within-quadrant areas and relative lack of activity that extends across the meridians.

Correlated Variability During WM Maintenance

Although the previous results reveal that WM representations of visual space are nonlinearly biased by meridians, they do not inform us about the mechanisms underlying this bias. It is thought that the sustained activity encoding visuospatial WM is maintained by a neural circuit structure characterized by recurrent excitatory connections between similarly-tuned neurons and lateral inhibitory connections between dissimilarly-tuned neurons (Zipser et al. 1993; Batuev 1994; Goldman-Rakic 1995; Camperi and Wang 1998; Compte et al. 2000; Durstewitz et al. 2000; Constantinidis and Wang 2004; Compte 2006). One prediction of this connection scheme is that correlated variability in firing rate should be greater between similarly tuned neurons than dissimilarly tuned neurons. Accordingly, the correlated variability between pairs of neurons encoding visuospatial WM representations in the same quadrant (intraquadrant pairs) should be

greater than between neurons encoding representations in different quadrants (extraquadrant pairs).

We found that the relationship between tuning similarity and spike count correlation (r_{sc} —a measure of correlated variability—see Methods) varies depending on the task epoch. During fixation, the magnitude of r_{sc} roughly followed the neuron pairs’ tuning similarity (Fig. 5A). Median r_{sc} was significantly greater than zero for intraquadrant pairs (Fig. 5A, red; $P < 0.05$, sign test, Hochberg-corrected), and for pairs with response peaks in the same left–right hemifield but different top–bottom hemifield (Fig. 5A, purple; $P < 0.05$, sign test, Hochberg-corrected). Median r_{sc} between intraquadrant neurons was also significantly higher than between neurons with response peaks across both meridians (i.e., the diagonally opposite quadrant; Fig. 5A; $P < 0.05$, Wilcoxon rank-sum test, Hochberg-corrected). During the stimulus epoch, median r_{sc} was not significantly different from zero for most tuning similarity groups (Fig. 5C; $P > 0.05$, sign test, Hochberg-corrected), and no groups were significantly different from each other (Fig. 5C; $P > 0.05$, Wilcoxon rank-sum test; Hochberg-corrected). We found that median r_{sc} during the delay epoch between intraquadrant neuron pairs was significantly greater than median r_{sc} between neurons with response peaks on the same side of the vertical meridian but opposite sides of the horizontal meridian (Fig. 5E; $P = 0.012$, Wilcoxon rank-sum test, Hochberg-corrected). This difference was absent for neurons with response peaks on opposite sides of the vertical meridian.

It is noteworthy that the predicted relationship between r_{sc} and the distance between response peaks was only visible within a left/right hemifield but not between left/right hemifields, which may reflect the independence of WM resources for the left and right hemifields (Buschman et al. 2011). Furthermore, these effects are not ascribable to differential responses to stimulus inputs, nor to differences in baseline firing rate of constituent neurons in a correlation pair, because r_{sc} are computed in a manner that control for these factors (see Methods). Thus, we consider these effects to result from the underlying network architecture and not from firing rate or stimulus-driven effects.

Quadratic Bias in Single-Trial Ensemble Representations

Given that single neuron firing rates for different remembered locations within quadrants were more similar to each other than locations between quadrants, it follows that dlPFC ensemble representations of within-quadrant locations should be more similar than across-quadrant representations. To test this hypothesis, we decoded the remembered stimulus location from ensembles of simultaneously recorded neurons on a single-trial basis using a

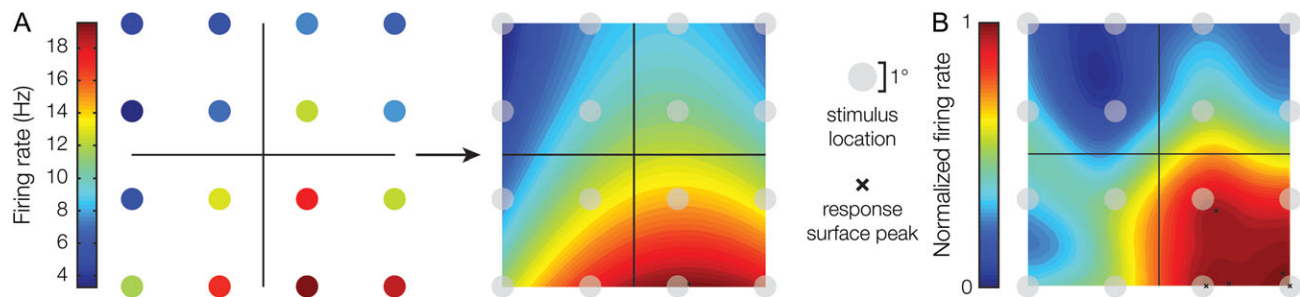


Figure 4. Visualizing the quadratic bias. (A) “Response surfaces” were computed by fitting a 2D, second-order polynomial to the mean firing rate for each of the 16 locations (see Methods). The resulting surface provides a continuous estimation of the neuron’s response to the portion of the visual field covered by the stimulus array. (B) By superimposing the response surfaces of 5 single neurons, the quadratic bias in firing rates becomes clearly visible. Notice the restriction of neural activity to within-quadrant areas and relative lack of activity that extends beyond quadrants. X’s indicate the peaks of each of the 5 neurons included in this panel.

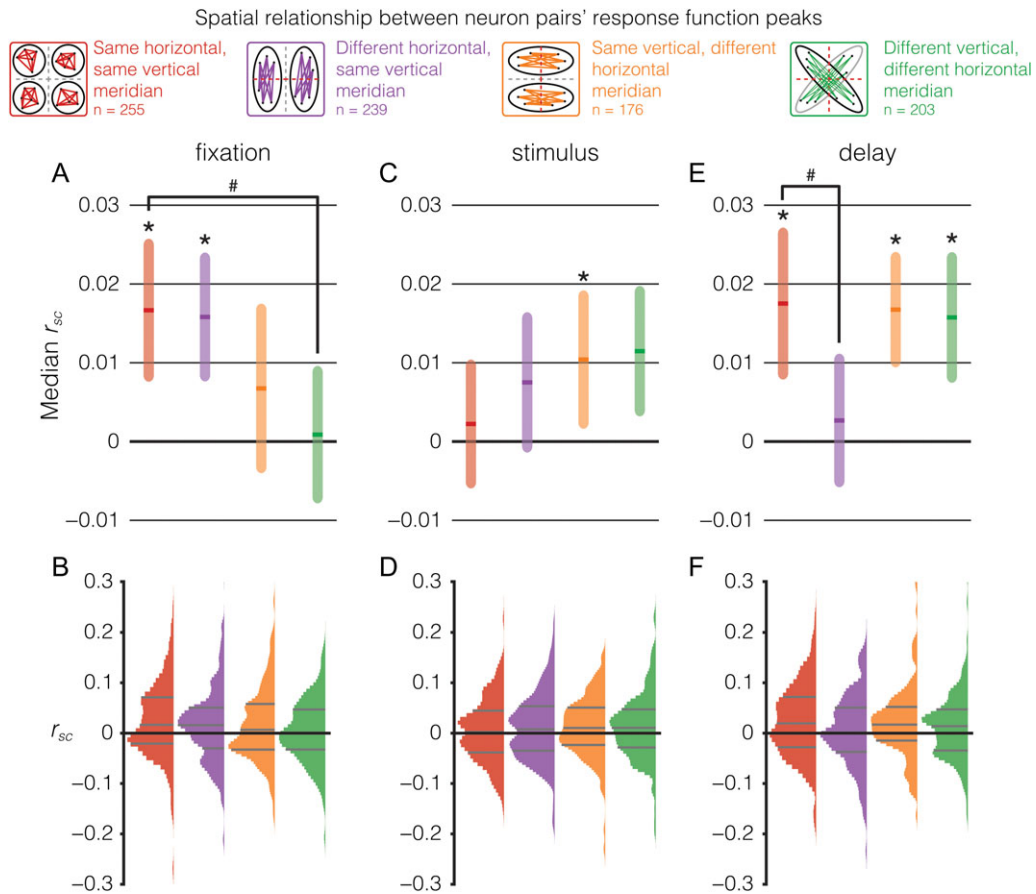


Figure 5. Correlated variability across task epochs. (A) Median r_{sc} (y-axis) between delay-selective neurons during the fixation epoch, grouped based on tuning similarity (x-axis). Tuning similarity is determined based on the relative spatial relationship between the quadrants that contain the constituent neurons' response peaks. The legend at the top of the figure depicts each spatial relationship category, showing response peak locations for example correlation pairs in that category. The shaded region is the 95% confidence intervals of the median. *Median different from 0, $P < 0.05$, Sign test, Hochberg-corrected. # $P < 0.05$, Wilcoxon rank-sum test, Hochberg-corrected. (B) r_{sc} distributions for each tuning similarity group in (A). Grey lines denote 25th, 50th (i.e., median), and 75th percentiles. Values of $r_{sc} > 0.3$ or < -0.3 , which constitute less than 5% of the distributions, are omitted from the plot. (C) Same as (A), but for the stimulus epoch. (D) Same as (B), but for the stimulus epoch. (E) Same as (A), but for the delay epoch. (F) Same as (B), but for the delay epoch.

machine-learning algorithm (SVM, see Methods (Cortes and Vapnik 1995)) as in Leavitt et al. (2017). This method is well-suited to decoding the high-dimensional representations of large groups of neurons (Rigotti et al. 2013; Moreno-Bote et al. 2014).

If population representations of visual-mnemonic space have lower resolution within a quadrant than across quadrants, the decoder should commit intraquadrant classification errors with greater probability than extraquadrant classification errors. Indeed, this is exactly what our data show ($P < 0.001$, χ^2 test, Hochberg-corrected; Fig. 6A). The probability of committing an erroneous intraquadrant classification is approximately twice that of committing an erroneous extraquadrant classification. We found a similar quadrantic bias in the ensemble representation during the stimulus epoch (Fig. 6B); however, the effect was significantly stronger during the delay epoch. The odds ratio of intraquadrant: extraquadrant decoding errors was significantly greater during the delay epoch compared with the stimulus epoch (Fig. 6C; $P < 0.01$, z-test). As with the single neuron firing rate data, we also analyzed each meridian and stimulus eccentricity configuration separately, and found that the effect was present in all combinations during memory and some combinations during stimulus presentation (Fig. S6). These results indicate that ensemble-level representations of a given location are more similar to the representations of other

intraquadrant locations than equidistant extraquadrant locations, and that this bias is stronger during memory maintenance than during sensory input.

Quadrantic Biases in Behavior

Given that we observed significant effects of intraquadrant versus extraquadrant visuospatial mnemonic representations on firing rates, ensemble coding, and spike-rate correlations, we wanted to know whether these effects also manifest in the animals' behavior. We hypothesized that because intraquadrant representations have lower resolution than extraquadrant representations, this should systematically bias memory-guided saccade endpoints toward quadrants and away from meridians, an effect previously reported in human and monkey psychophysical studies (Huttenlocher et al. 1991, 2004; Merchant et al. 2004; Haun et al. 2005). We tested this hypothesis by using the 4 target locations as outer boundaries to delineate a square region within a quadrant, and calculated the proportion of saccades that fell within that square region (Fig. 7A). If saccades are not systematically drawn toward quadrant centers, only 25% of saccade endpoints should fall in this square region, whereas if saccades are biased toward quadrant centers, more than 25% of saccades should fall within this region.

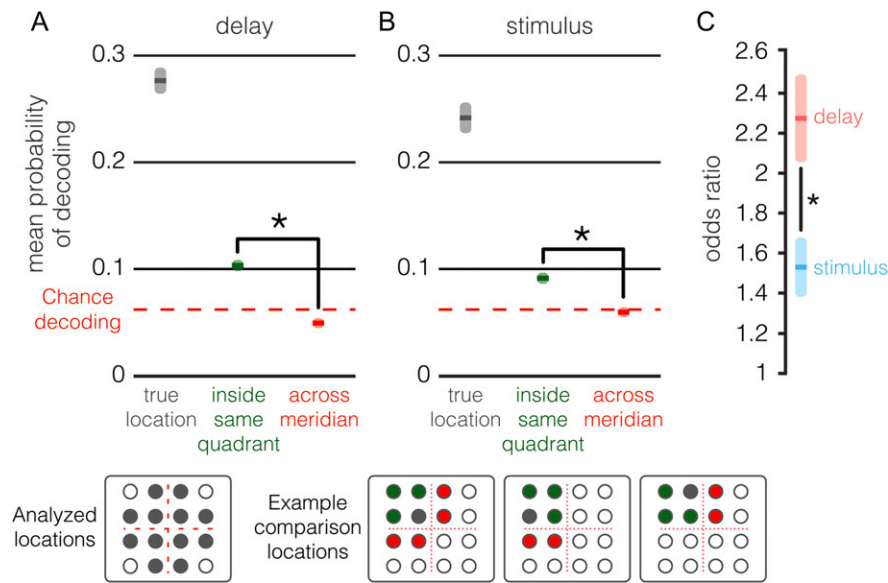


Figure 6. Quadrantic bias in ensemble representation. (A) Mnemonic representations were decoded from ensembles of simultaneously recorded neurons during the delay epoch. The probability of correctly decoding the remembered location during the delay epoch (grey), erroneously decoding it as an intraquadrant location (green), and erroneously decoding it as an extraquadrant location (red), pooled across all locations that lie adjacent to a meridian. Note that this analysis controls for the different proportion of intraquadrant versus the extraquadrant locations. Shaded regions indicate 95% confidence intervals of the proportion. * $P < 0.001$, χ^2 test, Hochberg-corrected. (B) Same as (A), but for the stimulus epoch. (C) The odds ratio of intraquadrant: extraquadrant decoding errors is plotted for the delay (red) and stimulus (blue) epochs. Shaded regions indicate 99% confidence intervals. * $P < 0.01$, z-test, Hochberg-corrected.

We found that saccades were systematically attracted toward quadrant centers in all 4 quadrants when the data from both subjects were pooled (Fig. 7B; $P < 0.05$, z-test, Hochberg-corrected). However, the strength of the bias was heterogeneous across individual subjects. One subject robustly exhibited a quadrantic saccade bias in all 4 quadrants (Fig. 7D), but the other exhibited the bias in only 2 of 4 quadrants (Fig. 7F). Thus, the quadrantic biases that we observed in measurements of neural activity are also reflected in the animals' behavior similarly to previous findings in human and nonhuman primates, though we observed substantial variability across individuals.

Prior studies have found that biases in memory-based estimates of spatial location are more pronounced for longer memory delays (White et al. 1994; Merchant et al. 2004). In order to determine whether this effect was present in our data, we split the trials into 2 groups based on the duration of the memory delay: short trials, in which the memory delay was ≤ 1000 ms, and long trials, in which the memory delay was > 1000 ms. We compared the strength of the quadrantic bias in saccades in the short versus long memory delay trials, and did not find a significant difference between the 2 groups in any of the 4 quadrants (Supplementary Fig. S7; $P > 0.05$, χ^2 test, Hochberg-corrected).

It is possible that even if we could not detect an effect of memory delay duration on the quadrantic bias at the behavioral level, it could still be present at the neuronal level. However, a comparison the early delay epoch—defined as 151–450 ms after the beginning of delay epoch—and the late delay epoch—defined as the final 200 ms of the delay epoch—did not reveal any major differences in the strength of the quadrantic bias in the single neuron firing rates (Supplementary Figs. S8 and S9). The number of significant differences between responses to intraquadrant and extraquadrant locations and the pattern of significant differences were similar during the early and late delay epoch. It is possible that we failed to find a significant effect of delay epoch duration on the strength of the quadrantic bias because our

maximum delay duration was 1500 ms, while prior studies used delay durations of up to 5600 ms.

Discussion

We systematically varied the position of a remembered location across multiple dimensions of visual space in an oculomotor delayed-response task while simultaneously recording from ensembles of single neurons in dLPFC area 8a. We found a quadrant-centric bias of visual-mnemonic space representations, evident in single neuron firing rates, pairwise correlated variability, ensemble encoding of remembered location, and a bias in saccade endpoint towards quadrant centers. We also found that mnemonic activity is anatomically organized and clustered across dLPFC in a manner that partially reflects the geometric properties of visual space, but is not retinotopic.

Clustering of Mnemonic Representations in dLPFC

While there are abundant examples of topographic organization in brain regions more directly involved in sensory and motor processing, evidence for topography in dLPFC has historically been limited. This is likely because the basic sensory quantities under investigation in mapping studies do not have a straightforward relationship with the structure and function of dLPFC, a region known to be involved in comparatively abstract components of sophisticated behavior (Miller and Cohen 2001). One study found that receptive fields for visual stimuli tend to become larger and more eccentric as one moves dorsally, away from the ventral portion of the arcuate sulcus (Suzuki and Azuma 1983). Given the heterogeneity of individual samples and subjects in the trend they observed, the distribution of visual and mnemonic preferred location we report does not appear at odds with their findings.

A recent study by Kiani et al. (2015) took a novel approach to investigating electrophysiological topography in dLPFC. Also

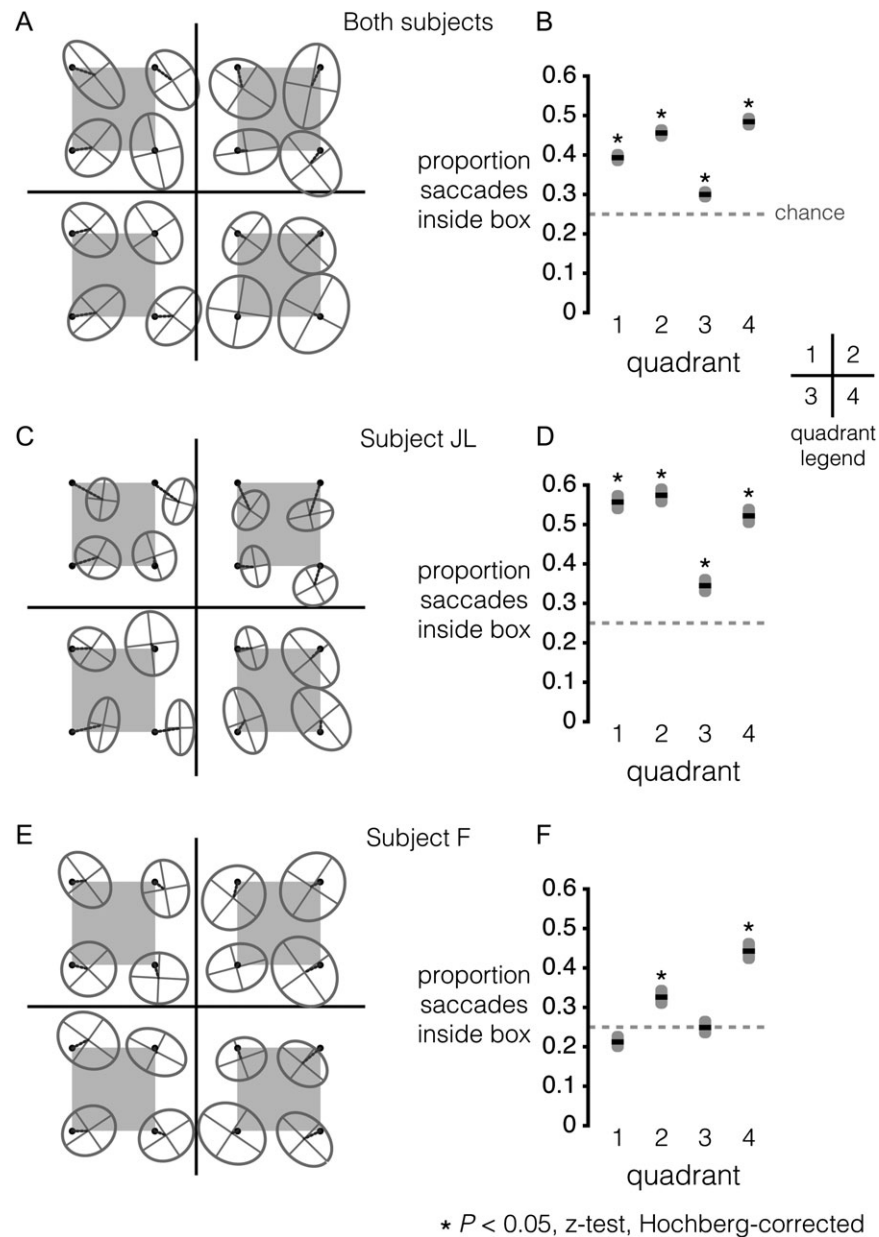


Figure 7. Saccades attract to quadrant centers. (A) Distributions of saccade endpoints for both subjects. The black dots denote the target locations, and the vertical and horizontal black lines represent the vertical and horizontal meridians, respectively. We calculated the elliptic bivariate normal distribution of the saccadic endpoints for each target (see Methods). The ellipse is centered at the x - y mean of the endpoints, and the length of the major and minor axes scaled to 95% of the distribution. A dotted line connects the target location to the center of the saccade endpoint distribution in order to visualize the difference between the 2 points. If significantly more than 25% of saccade endpoints fall within the grey box, we consider the quadrant center to act as an attractor for saccades (see Results). (B) Proportion of both subjects' saccades falling inside the grey box (y-axis) for each quadrant (x-axis). Shaded regions indicate 95% confidence intervals of the proportion. * $P < 0.01$, z-test. $n = 1442, 1457, 1431$, and 1412 , for quadrants 1, 2, 3, and 4, respectively. (C,D) Same as (A,B), but for subject JL. $n = 756, 763, 757$, and 755 , for quadrants 1, 2, 3, and 4, respectively. (E,F) Same as (A,B), but for subject F. $n = 686, 694, 674$, and 657 , for quadrants 1, 2, 3, and 4, respectively.

using microelectrode arrays implanted in area 8a, they applied techniques similar to those used in determining resting state networks in fMRI experiments, and grouped neurons into modules based on shared variability in firing rate across entire sessions of experimental recordings. They found that the modules were anatomically distinct, and organized more on the basis of “common noise” than on task-related activity, even across different tasks. Given the difference in analytical techniques between their study and ours, it does not seem that the 2 sets of findings necessitate reconciliation. Indeed, considering our

results together with theirs leads to a potential conclusion that task-related properties of neurons cluster independently or are embedded within the modules that emerge as a result of intrinsic or task-independent variability.

Spatial representations are retinotopically organized across many primate visual areas (Van Essen et al. 1984; Maunsell and Van Essen 1987). However, our data do not show such a strict organization within the area covered by the microelectrode arrays, despite the fact that we found nonrandom representation of the entire stimulus array distributed across the area.

This strongly suggests that such a retinotopic organization is absent in the dLPFC. One possible explanation for this finding is that interactions between neurons representing different locations across the visual space through lateral connections are facilitated by the heterogeneity within a relative retinotopic arrangement. Supporting this claim, lateral connections between neurons in the dLPFC are limited to a few millimeters (Kritzer and Goldman-Rakic 1995), and such connections may be critical to the implementation of delay activity dynamics during WM maintenance by ensembles of neurons (e.g., recurrent excitation and mutual inhibition) (Goldman-Rakic 1995). Prior work from our laboratory has also found that networks of dLPFC neurons that maximize WM-related information span a larger anatomical area than predicted by the statistics of a randomly-sampled neuronal population (Leavitt et al. 2017). Our findings are also concordant with previous work indicating that the structure of spike count correlations seem to reflect a proposed coding scheme for WM networks in which narrow range excitation and wider range inhibition are critical to the maintenance of the representations (Camperi and Wang 1998; Compte et al. 2000; Leavitt et al. 2013).

Potential Origins of Quadrantic Biases in Visual and Mnemonic Space

Previous studies investigating meridian effects in WM have typically focused on WM capacity independence between the left and right hemifields, and all found some degree of hemifield independence at behavioral and/or physiological levels (Vogel and Machizawa 2004; Delvenne 2005; Buschman et al. 2011; Delvenne et al. 2011; Matsushima and Tanaka 2014). Although these experiments were designed to address WM capacity, their results can be interpreted as demonstrating a vertical meridian effect in visual-mnemonic space, albeit within a context constrained by a binary parameterization of the space. Our results demonstrate the existence of a vertical meridian effect in a more sophisticated model of visual-mnemonic space, and specify the spatial structure and variability of this phenomenon.

We found that mnemonic representations of a given location are more similar to other locations within the same quadrant than to equidistant locations that lie across a meridian, at both the single neuron and population levels. One interpretation of this finding is that visual and memory fields adjacent to a meridian extend further in the same quadrant in which the field's epicenter is located than across the meridian. The literature on multidimensional visual and memory field characteristics of neurons in area 8a is limited (Rainer et al. 1998).

It is possible that the biases in the representations of visuo-mnemonic space reported here result from biases in the structure of receptive fields in areas upstream from dLPFC area 8a. For example, receptive fields in visual striate and extrastriate areas are retinotopically organized, are constrained to the contralateral visual hemifield, and their size is smallest in the fovea and increases proportionally to eccentricity (Virsu and Rovamo 1979; Van Essen et al. 1984; Kandel et al. 2000). However, in areas downstream from unimodal visual cortices, such as the dLPFC, this organization changes. Neurons mainly respond to visual stimuli that are behaviorally relevant, and receptive fields are located in both visual hemifields (Suzuki and Azuma 1983; Boch and Goldberg 1989). Interestingly, bilateral representation of the visual field does not start de-novo in dLPFC; areas upstream along both the dorsal and ventral pathways, such as medial superior temporal (MST) and inferior

temporal (IT), also show bilateral receptive fields (Gross et al. 1969; Desimone et al. 1984; Komatsu and Wurtz 1988; Raiguel et al. 1997).

One possible explanation for the vertical meridian bias observed in our data is that the contralateral hemifield representation bias present in visual areas is "passed on" to neurons in area 8a. This explanation could be extended to the observed quadrantic bias, as vertical asymmetries (i.e., across the horizontal meridian) are known to exist along the visual system; a greater area of the LGN, V1, and MT are devoted to representing the inferior half of the visual field (Connolly and Van Essen 1984; Van Essen et al. 1984; Maunsell and Van Essen 1987). These anatomical properties have been proposed as the reason why spatial frequency perception is superior along the inferior portion of the vertical meridian relative to the superior portion, and the origin of the BOLD signal asymmetries in human V1 and V2 that mirror the behavioral phenomenon (Carrasco et al. 2001; Liu et al. 2006; Abrams et al. 2012).

It is surprising that the strength of the horizontal and vertical meridian effects are similar for neurons with central preferred locations, given the contralateral representation bias that is ubiquitous across the brain. It is still possible that this contralateral representation bias underlies the lack of a significant horizontal meridian effect for neurons with peripheral preferred locations. However, the lack of a significant effect could also be due to an insufficiently large sample of neurons; we obtained only 21 neurons with peripheral preferred locations along the horizontal meridian, compared with 42 neurons for the vertical meridian.

One may speculate that the bias in WM representations results directly from a bias in visual representations, perhaps due to the overlap in populations of neurons representing visual and mnemonic information (Supplementary Fig. S1) (Constantinidis et al. 2001a). This is plausible, but the increased strength of the quadrantic bias during the delay epoch relative to during stimulus presentation indicates that this explanation is incomplete, and that WM maintenance amplifies existing representational biases and/or creates novel ones entirely.

Another series of studies in humans and nonhuman primates posits that WM-based estimates of spatial location rely on 2 distinct processes: an unbiased fine-grain representation of visual space, and a categorical representation of a larger region bounded by landmarks or natural divisions in visual space (e.g., meridians) that encompasses the fine-grain values (Huttenlocher et al. 1991, 2004; Merchant et al. 2004; Haun et al. 2005). The fine-grain information is subject to temporal decay, and thus over longer memory delays the representation becomes biased toward category (the quadrant centers, in the present study). While such a system introduces bias, it can also reduce trial-to-trial variability to a degree that yields a net accuracy benefit. One experimentally verified prediction of this model is that the categorical bias grows stronger as the memory delay increases (Merchant et al. 2004). We did not observe this phenomenon in the behavior or the neuronal activity in the present experiment, which we ascribe to the length of the memory delay in our task. Our memory delay ranged from 494 to 1500 ms, while the memory delay in the prior study ranged from 500 to 5000 ms. It is likely that the strength of the bias did not change sufficiently to be detectable in our shorter time window. The limited time windows for analysis of single neuron firing rates could also have yielded noisier firing rate estimations that obscured an underlying difference. Nevertheless, given the PFC's involvement in WM and categorical representation of continuous quantities (Freedman and Miller 2008;

Merchant et al. 2011; Goodwin et al. 2012), further studies with longer memory delays may reveal neurophysiological correlates of the behavioral phenomena we were unable to find in the present study.

Distinction Between 8a and Frontal Eye Field

Although some may consider area 8a an extension of the FEFs, this may not be accurate. While only 10–20% of neurons in FEF exhibit ipsilateral selectivity (Bruce and Goldberg 1985; Bruce et al. 1985; Sommer and Wurtz 2000), a larger proportion of neurons in area 8a—up to 40%—have visual and memory fields located in the ipsilateral visual hemifield (Lennert and Martinez-Trujillo 2011, 2013; Bullock et al. 2017). Area 8a also has a well-defined granular layer, while FEF, located immediately posterior to 8a in the arcuate sulcus, is distinctly dysgranular (Petrides 2005a). Furthermore, microstimulation with low currents (<50 μ A) does not evoke saccades in area 8a, while it does in the FEF (Bruce et al. 1985; Schall et al. 1995; Petrides 2005a). Finally, we, along with other groups, have documented selectivity for nonspatial object features in 8a neurons (Miller and Cohen 2001; Hussar and Pasternak 2010; Mendoza-Halliday et al. 2014), while the same selectivity has not been found in FEF. Thus, the properties of area 8a neurons during visual and WM tasks cannot be reduced to the properties of FEF neurons.

It is puzzling that the FEF, considered downstream from MST and IT, primarily has receptive fields in the contralateral visual field. It may be that the FEF lies at a point in the visuomotor transformation process in which receptive fields “recover” their contralateral representational bias and revert to retinotopic organization. This could be a fundamental feature of information transmission to motor structures, as movement coding is usually restricted to effectors in the contralateral side of the body. Given that a hemifield bias similar to that found in FEF is also observed in the Superior Colliculus (Goldberg and Wurtz 1972a, 1972b; Wurtz and Goldberg 1972), this explanation is parsimonious with these areas’ position at the “motor” end of the visuomotor transformation.

However, it is unclear whether area 8a and FEF are serially connected in the stream of visuomotor processing. An alternative possibility is that association areas such as 8a utilize connections with other motor areas such as FEF to monitor and/or select between representations of sensory information and motor plans during complex tasks (Petrides 2005a, 2005b). Supporting this hypothesis, patients with prefrontal lesions do not show sensory or motor deficits in simple visuomotor tasks such as visually guided saccades, while they are strongly impaired when performing tasks that require contextual flexibility of behavior (Petrides 1982, 1987, 2005a, 2005b). Thus, within this framework, the dlPFC may play a role in tasks in which the transformation of sensory information into motor commands is not direct, but requires flexible behavior (Petrides 2005a; Fuster 2008). Anatomical and evolutionary evidence supports this hypothesis, as the dlPFC is one of the regions that has undergone the most significant relative size increases in primates, compared with other animals with less sophisticated behavioral repertoires (Fuster 2008).

Alternative Factors Affecting Memory-Guided Saccades

The amplitude of memory-guided saccades is known to be influenced by a number of factors, including illumination (Goffart et al. 2006), training (Visscher et al. 2003), and orbital position of the eyes (Barton and Sparks 2001), though it is

unlikely these factors significantly biased eye movement data in this experiment. Head orientation, the location of the subject relative to the screen, and the location of the fixation point on the screen were all constant within and across sessions, thus there should have been little variation in orbital position and its consequences on saccades (Barton and Sparks 2001) should be minimal. Subjects were tested on the same 16 locations throughout training and recording, thus the interactions between trained and novel remembered saccade targets described in Visscher et al. (2003) are not present in this experiment. While previous studies have reported an upward bias in memory-guided saccades that decreases with the vertical position of the target (Gnadt et al. 1991; White et al. 1994; Goffart et al. 2006), this effect is largely eliminated in the presence of dim illumination (6.5×10^{-3} – 0.05 cd/m²) (Gnadt et al. 1991; Goffart et al. 2006) comparable to that generated by the projector in this task. As such, our experimental design seems to control for factors known to affect the amplitude of memory-guided saccades.

Meridian Effects Elucidate the Relationships Between WM, Attention, and Motor Activity

Substantial literature exists on the overlap and interaction between the behavioral effects and neural substrates of attention and WM (LaBar et al. 1999; Awh and Jonides 2001; de Fockert 2001; Miller and Cohen 2001; Lebedev et al. 2004; Awh et al. 2006; Postle 2006; Theeuwes et al. 2009; Ikkai and Curtis 2011; Mendoza et al. 2011; Gazzaley and Nobre 2012). Indeed, there is good reason to believe that much of the neural activity in dlPFC that is traditionally considered WM maintenance-related can instead be attributed to the attentional component of WM tasks (Owen et al. 1996; Lebedev et al. 2004). As such, our finding of quadrantic divisions of visual-mnemonic space could share neural origins with the quadrant-independent capacity for multiobject attention (Carlson et al. 2007) and the mitigating effects of meridians on visual crowding (Liu et al. 2009).

Perceptual biases relative meridians have been reported in previous behavioral studies. For example, it is well known that subjects overestimate the angle/direction relative to a meridian during orientation and motion direction discrimination tasks, a phenomenon known as motion or orientation repulsion (Loffler and Orbach 2001; Changizi et al. 2008; Dakin et al. 2010). This effect may be related to our findings that perceptual and mnemonic representations are “repulsed” away from main meridians.

Three decades ago, Rizzolatti et al. found that shifts of attention across a meridian cause substantially larger reaction time penalties than equidistant shifts of attention within a quadrant (Rizzolatti et al. 1987). This finding contributed to the basis of the premotor theory of attention (Rizzolatti et al. 1987; Sheliga et al. 1994). Many of the theory’s claims about the relationship between eye movements and attention have been called into question by later studies, yielding a refined version of the theory that is best summarized as “saccade preparation is necessary for exogenous attentional orienting, whereas endogenous attentional orienting is entirely independent of motor control” (Smith and Schenk 2012). Interestingly, meridian effects seem to only exist for endogenous attention and not exogenous attention (Reuter-Lorenz and Fendrich 1992; Botta et al. 2010). We consider the presence of mnemonic spatial meridian effects as evidence that dlPFC delay activity is not principally motor-related because, as mentioned before, meridian effects only exist for endogenous attention, which acts independently of motor control (Smith and Schenk 2012). Furthermore, because attentional meridian effects are only observed in endogenous attention, our

observation of quadratic biases in spatial WM representations specifies an overlap between WM and “endogenous” attention, not exogenous attention.

r_{sc} and WM Tasks

Previous studies in dLPFC have reported varying degrees of correlated activity during WM tasks (Funahashi and Inoue 2000; Constantinidis et al. 2001b; Constantinidis and Goldman-Rakic 2002; Funahashi 2006; Qi and Constantinidis 2012; Katsuki and Constantinidis 2013; Wimmer et al. 2014; Leavitt et al. 2017). A previous study from our laboratory analyzing some of the same data as this experiment (Leavitt et al. 2017) found that the mean r_{sc} was lower during the stimulus epoch than during fixation and the memory epochs, but that the fixation and memory epochs were not significantly different from one another. However, the relationship between neurons’ tuning similarity and r_{sc} changed between the fixation and memory epochs, indicating a change in the network structure. Furthermore, the r_{sc} structure could improve or impair WM coding, depending on the properties of the neuronal ensemble. Regarding the delay epoch specifically, one prior study found that cross-correlation strength and significance was positively correlated with tuning similarity during memory (Constantinidis et al. 2001b), another found a nonsignificant trend that task epoch affects r_{sc} (Constantinidis and Goldman-Rakic 2002), and a third demonstrated r_{sc} differences between animals naïve to and proficient at a spatial WM task (Qi and Constantinidis 2012). Recently, analysis by Wimmer et al. found that r_{sc} varied during memory in a tuning-dependent manner (Wimmer et al. 2014) indicative of a continuous “bump attractor” representation scheme (Compte et al. 2000) of spatial WM. We found a similar relationship between tuning and r_{sc} during the fixation epoch. However, we found that r_{sc} during the delay epoch only changes as a function of tuning for neurons that have preferred memory locations on the same side of the vertical meridian (i.e., within the same left-right hemifield). It is possible that the observed effects of tuning on r_{sc} in the aforementioned studies were dominated by the within-hemifield effect, which can be explained by the higher proportion of contralateral-selective neurons in this region (Funahashi and Kubota 1994; Goldman-Rakic 1995; Funahashi and Takeda 2002; Lennert and Martinez-Trujillo 2011, 2013; Bullock et al. 2017). The previous study from our laboratory also found that r_{sc} varies in a tuning-dependent manner across the fixation, stimulus, and delay epochs (Leavitt et al. 2017). That study quantified tuning similarity as the signal correlation (r_{signal}) between neurons, whereas the present study grouped neurons based on the spatial relationship of the quadrants containing the neurons’ fitted response peaks. This apparent discrepancy can be accounted for by the differences in the tuning similarity metrics, and the tendency of dLPFC neurons to exhibit nontraditional tuning functions (Constantinidis et al. 2002; Rigotti et al. 2013; Fusi et al. 2016). It also suggests that traditional measures of tuning similarity may be overly simplistic for accurately describing the multidimensional representations of PFC ensembles (Fusi et al. 2016).

A Hemifield-Independent WM Mechanism

We found that r_{sc} during the delay epoch between intraquadrant neuron pairs was significantly larger than r_{sc} between neurons with response peaks in the same left-right hemifield and in different top-bottom hemifields. However, we did not find any significant difference in r_{sc} between neuron pairs with response peaks on opposite sides of the vertical meridian. Our

interpretation of this finding is that WM maintenance results in inhibition between neurons with response peaks in the same left-right hemifield and in different top-bottom hemifields. The finding that the horizontal meridian exerts the strongest effect on the r_{sc} structure can synthesize 2 well characterized, but previously unrelated findings regarding neuronal correlates and behavioral phenomena in WM. First, the existence of a model network architecture that stabilizes WM representations across time (Polk et al. 2012). One hallmark of this architecture is that correlated activity between neurons that maintain similar WM representations (e.g., locations within the same visual quadrant) is stronger than correlated activity between neurons that store different kinds of WMs (e.g., locations in different visual quadrants). Second, the finding of independent WM resources for the left and right hemifields of visual space (Delvenne 2005; Buschman et al. 2011; Alvarez et al. 2012; Matsushima and Tanaka 2014). Combining both of these factors yields the prediction that the correlation structure indicative of a WM-stabilizing architecture should be present separately for each left/right hemifield. Indeed, our data match this prediction, advancing a model of WM that integrates a model network architecture with known behavioral and neural biases.

Conclusion

Our results indicate that dLPFC contains a nonretinotopic, topographic organization of spatial WM representations likely shaped to support interactions between neurons that are essential to the origin of delay activity in the absence of visual inputs. This is supported by our observation of a pattern of correlated variability that is thought to be a hallmark of a mechanism for temporally stabilizing WM representations. Our results also provide a neural correlate for known quadratic biases in human and monkey visuospatial WM. Finally, our results suggest revisiting current models of WM to accommodate the nonlinearities of visual-mnemonic space representation in dLPFC.

Supplementary Material

Supplementary material is available at *Cerebral Cortex* online.

Authors’ Contributions

M.L.L., F.P., A.J.S., and J.C.M.T. designed the experiment, A.J.S. and J.C.M.T. conducted the surgeries, M.L.L. carried out the experiment with guidance from F.P., A.J.S. and J.C.M.T., M.L.L. analyzed the data, M.L.L. and J.C.M.T. prepared the manuscript.

Funding

This research was supported by the Canadian Institutes of Health Research and Natural Sciences and Engineering Research Council of Canada.

Notes

The authors would like to thank M. Schneiderman, W. Kucharski, and S. Nuara for technical assistance, the M.T. Lab and T. Quail for their scrutiny and mirth, and R. Gulli for providing a successful heading. *Conflict of Interest:* None declared.

References

- Abrams J, Nizam A, Carrasco M. 2012. Isoeccentric locations are not equivalent: the extent of the vertical meridian asymmetry. *Vision Res.* 52:70–78.
- Alvarez GA, Gill J, Cavanagh P. 2012. Anatomical constraints on attention: hemifield independence is a signature of multifocal spatial selection. *J Vis.* 12:9–9.
- Averbeck BB, Lee D. 2006. Effects of noise correlations on information encoding and decoding. *J Neurophysiol.* 95:3633–3644.
- Awh E, Jonides J. 2001. Overlapping mechanisms of attention and spatial working memory. *Trends Cogn Sci (Regul Ed).* 5:119–126.
- Awh E, Vogel EK, Oh SH. 2006. Interactions between attention and working memory. *Neuroscience.* 139:201–208.
- Baddeley AD, Hitch G. 1974. Working memory. In: Bower GH, editor. *The psychology of learning and motivation: advances in research and theory.* Vol. 8. New York: Academic Press. p. 47–89.
- Barton EJ, Sparks DL. 2001. Saccades to remembered targets exhibit enhanced orbital position effects in monkeys. *Vision Res.* 41:2393–2406.
- Batuev AS. 1986. Neuronal mechanisms of goal-directed behavior in monkeys. *Neurosci Behav Physiol.* 16:459–465.
- Batuev AS. 1994. Two neuronal systems involved in short-term spatial memory in monkeys. *Acta Neurobiol Exp (Wars).* 54:335–344.
- Boch RA, Goldberg ME. 1989. Participation of prefrontal neurons in the preparation of visually guided eye movements in the rhesus monkey. *J Neurophysiol.* 61:1064–1084.
- Botta F, Santangelo V, Raffone A, Lupiáñez J, Belardinelli MO. 2010. Exogenous and endogenous spatial attention effects on visuospatial working memory. *Q J Exp Psychol (Hove).* 63:1590–1602.
- Boulay CB, Pieper F, Leavitt M, Leavitt M, Sachs AJ. 2016. Single-trial decoding of intended eye movement goals from lateral prefrontal cortex neural ensembles. *J Neurophysiol.* 115:486–499.
- Bruce CJ, Goldberg ME. 1985. Primate frontal eye fields. I. Single neurons discharging before saccades. *J Neurophysiol.* 53:603–635.
- Bruce CJ, Goldberg ME, Bushnell MC, Stanton GB. 1985. Primate frontal eye fields. II. Physiological and anatomical correlates of electrically evoked eye movements. *J Neurophysiol.* 54:714–734.
- Bullock KR, Pieper F, Sachs AJ, Martinez-Trujillo JC. 2017. Visual and presaccadic activity in area 8Ar of the macaque monkey lateral prefrontal cortex. *J Neurophysiol.* doi: 10.1152/jn.00278.2016.
- Buschman TJ, Siegel M, Roy JE, Miller EK. 2011. Neural substrates of cognitive capacity limitations. *PNAS.* 108:11252–11255.
- Camperi M, Wang XJ. 1998. A model of visuospatial working memory in prefrontal cortex: recurrent network and cellular bistability. *J Comput Neurosci.* 5:383–405.
- Carlson TA, Alvarez GA, Cavanagh P. 2007. Quadrantic deficit reveals anatomical constraints on selection. *PNAS.* 104:13496–13500.
- Carrasco M, Talgar CP, Cameron EL. 2001. Characterizing visual performance fields: effects of transient covert attention, spatial frequency, eccentricity, task and set size. *Spat Vis.* 15:61–75.
- Chang CC, Lin CJ. 2011. LIBSVM: a library for support vector machines. *ACM Trans Intell Syst Technol (TIST).* 2:27.
- Changizi MA, Hsieh A, Nijhawan R, Kanai R, Shimojo S. 2008. Perceiving the present and a systematization of illusions. *Cogn Sci.* 32:459–503.
- Cohen MR, Kohn A. 2011. Measuring and interpreting neuronal correlations. *Nat Neurosci.* 14:811–819.
- Compte A. 2006. Computational and in vitro studies of persistent activity: edging towards cellular and synaptic mechanisms of working memory. *Neuroscience.* 139:135–151.
- Compte A, Brunel N, Goldman-Rakic PS, Wang X-J. 2000. Synaptic mechanisms and network dynamics underlying spatial working memory in a cortical network model. *Cereb Cortex.* 10:910–923.
- Connolly M, Van Essen D. 1984. The representation of the visual field in parvocellular and magnocellular layers of the lateral geniculate nucleus in the macaque monkey. *J Comp Neurol.* 226:544–564.
- Constantinidis C, Franowicz MN, Goldman-Rakic PS. 2001b. Coding specificity in cortical microcircuits: a multiple-electrode analysis of primate prefrontal cortex. *J Neurosci.* 21:3646–3655.
- Constantinidis C, Franowicz MN, Goldman-Rakic PS. 2001a. The sensory nature of mnemonic representation in the primate prefrontal cortex. *Nat Neurosci.* 4:311–316.
- Constantinidis C, Goldman-Rakic P. 2002. Correlated discharges among putative pyramidal neurons and interneurons in the primate prefrontal cortex. *J Neurophysiol.* 88:3487–3497.
- Constantinidis C, Procyk E. 2004. The primate working memory networks. *Cogn Affect Behav Neurosci.* 4:444–465.
- Constantinidis C, Wang X-J. 2004. A neural circuit basis for spatial working memory. *Neuroscientist.* 10:553–565.
- Constantinidis C, Williams GV, Goldman-Rakic PS. 2002. A role for inhibition in shaping the temporal flow of information in prefrontal cortex. *Nat Neurosci.* 5:175–180.
- Cortes C, Vapnik V. 1995. Support-vector networks. *Mach Learn.* 20:273–297.
- Dakin SC, Athorp D, Alais D. 2010. Anisotropies in judging the direction of moving natural scenes. *J Vis.* 10:5.
- de Fockert JW. 2001. The role of working memory in visual selective attention. *Science.* 291:1803–1806.
- Delvenne J-F. 2005. The capacity of visual short-term memory within and between hemifields. *Cognition.* 96:B79–B88.
- Delvenne J-F, Kaddour LA, Castronovo J. 2011. An electrophysiological measure of visual short-term memory capacity within and across hemifields. *Psychophysiology.* 48:333–336.
- Desimone R, Albright TD, Gross CG, Bruce C. 1984. Stimulus-selective properties of inferior temporal neurons in the macaque. *J Neurosci.* 4:2051–2062.
- Durstewitz D, Seamans JK, Sejnowski TJ. 2000. Neurocomputational models of working memory. *Nat Neurosci.* 3:1184–1191.
- Engle RW, Tuholski SW, Laughlin JE, Conway AR. 1999. Working memory, short-term memory, and general fluid intelligence: a latent-variable approach. *J Exp Psychol Gen.* 128:309–331.
- Freedman DJ, Miller EK. 2008. Neural mechanisms of visual categorization: insights from neurophysiology. *Neurosci Biobehav Rev.* 32:311–329.
- Funahashi S. 2006. Prefrontal cortex and working memory processes. *Neuroscience.* 139:251–261.
- Funahashi S, Bruce C, Goldman-Rakic PS. 1989. Mnemonic coding of visual space in the monkey's dorsolateral prefrontal cortex. *J Neurophysiol.* 61:331–349.
- Funahashi S, Inoue M. 2000. Neuronal interactions related to working memory processes in the primate prefrontal cortex revealed by cross-correlation analysis. *Cereb Cortex.* 10:535–551.

- Funahashi S, Kubota K. 1994. Working memory and prefrontal cortex. *Neurosci Res.* 21:1–11.
- Funahashi S, Takeda K. 2002. Information processes in the primate prefrontal cortex in relation to working memory processes. *Rev Neurosci.* 13:313–345.
- Fusi S, Miller EK, Rigotti M. 2016. Why neurons mix: high dimensionality for higher cognition. *Curr Opin Neurobiol.* 37:66–74.
- Fuster J. 2008. *The prefrontal cortex.* 4th ed. London: Elsevier.
- Fuster JM. 1973. Unit activity in prefrontal cortex during delayed-response performance: neuronal correlates of transient memory. *J Neurophysiol.* 36:61–78.
- Fuster JM, Alexander GE. 1971. Neuron activity related to short-term memory. *Science.* 173:652–654.
- Gazzaley A, Nobre AC. 2012. Top-down modulation: bridging selective attention and working memory. *Trends Cogn Sci (Regul Ed).* 16:129–135.
- Gnadt JW, Andersen RA. 1988. Memory related motor planning activity in posterior parietal cortex of macaque. *Exp Brain Res.* 70:216–220.
- Gnadt JW, Bracewell RM, Andersen RA. 1991. Sensorimotor transformation during eye movements to remembered visual targets. *Vision Res.* 31:693–715.
- Goffart L, Quinet J, Chavane F, Masson GS. 2006. Influence of background illumination on fixation and visually guided saccades in the rhesus monkey. *Vision Res.* 46:149–162.
- Goldberg ME, Wurtz RH. 1972a. Activity of superior colliculus in behaving monkey. I. Visual receptive fields of single neurons. *J Neurophysiol.* 35:542–559.
- Goldberg ME, Wurtz RH. 1972b. Activity of superior colliculus in behaving monkey. II. Effect of attention on neuronal responses. *J Neurophysiol.* 35:560–574.
- Goldman-Rakic PS. 1995. Cellular basis of working memory. *Neuron.* 14:477–485.
- Goodwin SJ, Blackman RK, Sakellaridi S, Chafee MV. 2012. Executive control over cognition: stronger and earlier rule-based modulation of spatial category signals in prefrontal cortex relative to parietal cortex. *J Neurosci.* 32:3499–3515.
- Gross CG, Bender DB, Rocha-Miranda CE. 1969. Visual receptive fields of neurons in inferotemporal cortex of the monkey. *Science.* 166:1303–1306.
- Haun DBM, Allen GL, Wedell DH. 2005. Bias in spatial memory: a categorical endorsement. *Acta Psychol (Amst).* 118:149–170.
- Hebb DO. 2005. *The organization of behavior: a neuropsychological theory.* New York: John Wiley & Sons.
- Hussar C, Pasternak T. 2010. Trial-to-trial variability of the prefrontal neurons reveals the nature of their engagement in a motion discrimination task. *PNAS.* 107:21842–21847.
- Huttenlocher J, Hedges LV, Corrigan B, Crawford LE. 2004. Spatial categories and the estimation of location. *Cognition.* 93:75–97.
- Huttenlocher J, Hedges LV, Duncan S. 1991. Categories and particulars: prototype effects in estimating spatial location. *Psychol Rev.* 98:352–376.
- Ikkai A, Curtis CE. 2011. Common neural mechanisms supporting spatial working memory, attention and motor intention. *Neuropsychologia.* 49:1428–1434.
- Kandel ER, Schwartz JH, Chao J. 2000. *Principles of neural science.* 4th ed. New York: McGraw-Hill.
- Katsuki F, Constantinidis C. 2013. Time course of functional connectivity in primate dorsolateral prefrontal and posterior parietal cortex during working memory. *PLoS One.* 8:e81601.
- Kiani R, Cueva CJ, Reppas JB, Peixoto D, Ryu SI, Newsome WT. 2015. Natural grouping of neural responses reveals spatially segregated clusters in prearcuate cortex. *Neuron.* 85:1359–1373.
- Komatsu H, Wurtz RH. 1988. Relation of cortical areas MT and MST to pursuit eye movements. I. Localization and visual properties of neurons. *J Neurophysiol.* 60:580–603.
- Kritzer MF, Goldman-Rakic PS. 1995. Intrinsic circuit organization of the major layers and sublayers of the dorsolateral prefrontal cortex in the rhesus monkey. *J Comp Neurol.* 359:131–143.
- LaBar KS, Gitelman DR, Parrish TB, Mesulam M. 1999. Neuroanatomic overlap of working memory and spatial attention networks: a functional MRI comparison within subjects. *Neuroimage.* 10:695–704.
- Leavitt ML, Pieper F, Sachs A, Joober R, Martinez-Trujillo JC. 2013. Structure of spike count correlations reveals functional interactions between neurons in dorsolateral prefrontal cortex area 8a of behaving primates. *PLoS One.* 8:e61503.
- Leavitt ML, Pieper F, Sachs AJ, Martinez-Trujillo JC. 2017. Correlated variability modifies working memory fidelity in primate prefrontal neuronal ensembles. *PNAS.* 114:E2494–E2503.
- Lebedev MA, Messinger A, Kralik JD, Wise SP. 2004. Representation of attended versus remembered locations in prefrontal cortex. *PLoS Biol.* 2:e365.
- Lennert T, Martinez-Trujillo JC. 2011. Strength of response suppression to distracter stimuli determines attentional-filtering performance in primate prefrontal neurons. *Neuron.* 70:141–152.
- Lennert T, Martinez-Trujillo JC. 2013. Prefrontal neurons of opposite spatial preference display distinct target selection dynamics. *J Neurosci.* 33:9520–9529.
- Liu T, Heeger DJ, Carrasco M. 2006. Neural correlates of the visual vertical meridian asymmetry. *J Vis.* 6:1294–1306.
- Liu T, Jiang Y, Sun X, He S. 2009. Reduction of the crowding effect in spatially adjacent but cortically remote visual stimuli. *Curr Biol.* 19:127–132.
- Loffler G, Orbach HS. 2001. Anisotropy in judging the absolute direction of motion. *Vision Res.* 41:3677–3692.
- Matsushima A, Tanaka M. 2014. Different neuronal computations of spatial working memory for multiple locations within versus across visual hemifields. *J Neurosci.* 34:5621–5626.
- Maunsell JH, Van Essen DC. 1987. Topographic organization of the middle temporal visual area in the macaque monkey: representational biases and the relationship to callosal connections and myeloarchitectonic boundaries. *J Comp Neurol.* 266:535–555.
- Maynard EM, Nordhausen CT, Normann RA. 1997. The Utah intracortical electrode array: a recording structure for potential brain-computer interfaces. *Electroencephalogr Clin Neurophysiol.* 102:228–239.
- Mendoza D, Schneiderman M, Kaul C, Martinez-Trujillo J. 2011. Combined effects of feature-based working memory and feature-based attention on the perception of visual motion direction. *J Vis.* 11:11–11.
- Mendoza-Halliday D, Torres S, Martinez-Trujillo JC. 2014. Sharp emergence of feature-selective sustained activity along the dorsal visual pathway. *Nat Neurosci.* 17:1255–1262.
- Merchant H, Crowe DA, Robertson MS, Fortes AF, Georgopoulos AP. 2011. Top-down spatial categorization signal from prefrontal to posterior parietal cortex in the primate. *Front Syst Neurosci.* 5:69.
- Merchant H, Fortes AF, Georgopoulos AP. 2004. Short-term memory effects on the representation of two-dimensional space in the rhesus monkey. *Anim Cogn.* 7:133–143.

- Miller EK, Cohen JD. 2001. An integrative theory of prefrontal cortex function. *Annu Rev Neurosci.* 24:167–202.
- Moran PAP. 1950. Notes on continuous stochastic phenomena. *Biometrika.* 37:17–23.
- Moreno-Bote R, Beck J, Kanitscheider I, Pitkow X, Latham P, Pouget A. 2014. Information-limiting correlations. *Nat Neurosci.* 17:1410–1417.
- Niki H. 1974. Differential activity of prefrontal units during right and left delayed response trials. *Brain Res.* 70:346–349.
- Normann RA, Maynard EM, Rousche PJ, Warren DJ. 1999. A neural interface for a cortical vision prosthesis. *Vision Res.* 39:2577–2587.
- Owen AM, Evans AC, Petrides M. 1996. Evidence for a two-stage model of spatial working memory processing within the lateral frontal cortex: a positron emission tomography study. *Cereb Cortex.* 6:31–38.
- Petrides M. 1982. Motor conditional associative-learning after selective prefrontal lesions in the monkey. *Behav Brain Res.* 5:407–413.
- Petrides M. 1987. Conditional learning and the primate frontal cortex. In: Perecman E, editor. *The frontal lobes revisited.* New York: The IRBN Press. p. 91–108.
- Petrides M. 2005a. Lateral prefrontal cortex: architectonic and functional organization. *Proc R Soc B.* 360:781–795.
- Petrides M. 2005b. The rostral-caudal axis of cognitive control within the lateral frontal cortex. In: Dehaene S, Duhamel J-R, Hauser MD, Rizzolatti G, editors. *From monkey brain to human brain.* Cambridge: MIT Press. p. 293–314.
- Polk A, Litwin-Kumar A, Doiron B. 2012. Correlated neural variability in persistent state networks. *PNAS.* 109:6295–6300.
- Postle BR. 2006. Working memory as an emergent property of the mind and brain. *Neuroscience.* 139:23–38.
- Qi X-L, Constantinidis C. 2012. Correlated discharges in the primate prefrontal cortex before and after working memory training. *Eur J Neurosci.* 36:3538–3548.
- Raiguel S, Van Hulle MM, Xiao DK, Marcar VL, Lagae L, Orban GA. 1997. Size and shape of receptive fields in the medial superior temporal area (MST) of the macaque. *Neuroreport.* 8:2803–2808.
- Rainer G, Asaad WF, Miller EK. 1998. Memory fields of neurons in the primate prefrontal cortex. *PNAS.* 95:15008–15013.
- Rao SG, Williams GV, Goldman-Rakic PS. 1999. Isodirectional tuning of adjacent interneurons and pyramidal cells during working memory: evidence for microcolumnar organization in PFC. *J Neurophysiol.* 81:1903–1916.
- Reuter-Lorenz PA, Fendrich R. 1992. Oculomotor readiness and covert orienting: differences between central and peripheral precues. *Percept Psychophys.* 52:336–344.
- Rigotti M, Barak O, Warden MR, Wang X-J, Daw ND, Miller EK, Fusi S. 2013. The importance of mixed selectivity in complex cognitive tasks. *Nature.* 497:585–590.
- Riley MR, Constantinidis C. 2015. Role of prefrontal persistent activity in working memory. *Front Syst Neurosci.* 9:181.
- Rizzolatti G, Riggio L, Dascola I, Umiltà C. 1987. Reorienting attention across the horizontal and vertical meridians: evidence in favor of a premotor theory of attention. *Neuropsychologia.* 25:31–40.
- Schall JD, Morel A, King DJ, Bullier J. 1995. Topography of visual cortex connections with frontal eye field in macaque: convergence and segregation of processing streams. *J Neurosci.* 15:4464–4487.
- Sheliga BM, Riggio L, Rizzolatti G. 1994. Orienting of attention and eye movements. *Exp Brain Res.* 98:507–522.
- Smith DT, Schenk T. 2012. The Premotor theory of attention: time to move on? *Neuropsychologia.* 50:1104–1114.
- Sommer MA, Wurtz RH. 2000. Composition and topographic organization of signals sent from the frontal eye field to the superior colliculus. *J Neurophysiol.* 83:1979–2001.
- Suzuki H, Azuma M. 1983. Topographic studies on visual neurons in the dorsolateral prefrontal cortex of the monkey. *Exp Brain Res.* 53:47–58.
- Theeuwes J, Belopolsky A, Olivers CNL. 2009. Interactions between working memory, attention and eye movements. *Acta Psychol (Amst).* 132:106–114.
- Tremblay S, Pieper F, Sachs A, Leavitt M. 2014. Attentional filtering of visual information by neuronal ensembles in the primate lateral prefrontal cortex. *Neuron.* 85:202–215.
- Van Essen DC, Newsome WT, Maunsell JH. 1984. The visual field representation in striate cortex of the macaque monkey: asymmetries, anisotropies, and individual variability. *Vision Res.* 24:429–448.
- Virsu V, Rovamo J. 1979. Visual resolution, contrast sensitivity, and the cortical magnification factor. *Exp Brain Res.* 37:475–494.
- Visscher K, Viets E, Snyder LH. 2003. Effects of training on memory-guided saccade performance. *Vision Res.* 43:2061–2071.
- Vogel EK, Machizawa MG. 2004. Neural activity predicts individual differences in visual working memory capacity. *Nature.* 428:748–751.
- White JM, Sparks DL, Stanford TR. 1994. Saccades to remembered target locations: an analysis of systematic and variable errors. *Vision Res.* 34:79–92.
- Wimmer K, Nykamp DQ, Constantinidis C, Compte A. 2014. Bump attractor dynamics in prefrontal cortex explains behavioral precision in spatial working memory. *Nat Neurosci.* 17:431–439.
- Wurtz RH, Goldberg ME. 1972. Activity of superior colliculus in behaving monkey. III. Cells discharging before eye movements. *J Neurophysiol.* 35:575–586.
- Zipser D, Kehoe B, Littlewort G, Fuster J. 1993. A spiking network model of short-term active memory. *J Neurosci.* 13:3406–3420.
- Zuur A, Ieno EN, Smith GM. 2007. *Analysing ecological data.* New York: Springer.